Journal of MATERIALS RESEARCH

Article
DOI: 10.1557/jmr.2019.77

(NANO)MATERIALS FOR BIOMEDICAL APPLICATIONS

FOCUS ISSUE

Antimicrobial hydrogels with controllable mechanical properties for biomedical application

Si-Hao Chen[1,2], Zhi Li[1,2], Zu-Lan Liu[1,2], Lan Cheng[1,2,3], Xiao-Ling Tong[1,3], Fang-Yin Dai[1,2,3,a)]

[1]State Key Laboratory of Silkworm Genome Biology, Southwest University, Chongqing 400715, China
[2]Chongqing Engineering Research Center of Biomaterial Fiber and Modern Textile, College of Textile and Garment, Southwest University, Chongqing 400715, China
[3]Key Laboratory of Sericultural Biology and Genetic Breeding, Ministry of Agriculture, College of Biotechnology, Southwest University, Chongqing 400715, China
[a)]Address all correspondence to this author. e-mail: fydai@swu.edu.cn

Received: 2 December 2018; accepted: 11 February 2019

The antibacterial hydrogels can be widely used in the biomedical area owing to their excellent properties. The main limitation of antibacterial hydrogels is their poor mechanical strength. In this study, the novel hydrogels were fabricated with a mixture of silk fibroin (SF), chitosan (CH), agarose (AG), and silver nanoparticles (SNPs) via facile reaction condition without inorganic substances. The mechanical property of these fabricated hydrogels can be modulated by the concentration of SF or AG. The rheological studies demonstrated enhanced elasticity of CH-doped hydrogels. Because of the presence of CH and Ag in hydrogels, the antimicrobial property against gram-positive and gram-negative bacteria was exhibited. Cytocompatibility test proved the very low toxic nature of the hydrogels. In addition, these composite hydrogels have a smaller porosity, higher swelling ratio, and good compatibility, indicating their great potential for biomedical application.

Introduction

Skin, the tissue wrapping around muscle, is the largest organ in the human body with the function of protecting tissues and organs from physical, mechanical, chemical, and pathogenic injuries [1]. Skin injuries may cause tissue necrotization and hurt blood vessels, which will affect humans' health, even lives [2]. Cuticular wounds destroy the integrity of skin and their percolate is filled with abundant body fluid, making them more prone to bacterial infection [3]. A bacterial infection will delay wound healing and induce a scar. In recent years, many researches reveal that wound healing is faster in a humid environment than in a dry condition [4], since the suppression of cytoactive level could transform wounds into scab in a dry condition which will delay wound healing [5]. The articular cartilage is central to some pandemics such as osteoarthritis, playing an important biomechanical role as a load-bearing tissue, reducing joint friction. Unfortunately, this avascular, aneural, and alymphatic dense connective tissue is structurally predisposed to low self-regeneration capacity [6]. To solve these problems, various materials have been developed for preventing bacterial infection and accelerating the wound healing, including foam, membrane, and hydrogel.

Hydrogels, as the desired wound dressings, are a three-dimensional cross-linked polymer capable of absorbing and retaining large amounts of water [7, 8]. Hydrogels provide a highly mimetic environment of extracellular matrix and has excellent biocompatibility [9]. Because of their particular flexibility, hydrogels can closely contact with the surface of wounds [10]. Moreover, the high water content and good vapor permeability offer a good environment for wound healing [11]. Meanwhile, hydrogels can serve as active matrices to control cell morphology, proliferation, and differentiation [12]. Most importantly, the porous structure of hydrogels can effectively load antibacterial agents and then slowly release them into the wound surface to prevent infection [13]. Recent studies showed that hydrogels can be used as an ocular wound dressing, which can encapsulate and give sustained release of different antibiotics [14]. Agarose (AG), a neutral, galactopyranose-based

https://doi.org/10.1557/jmr.2019.77 Published online by Cambridge University Press

© Materials Research Society 2019

linear polysaccharide, is a biocompatible and readily available material that potentially offers a wide dynamic range of biophysical properties [15]. To address the limitation of pure AG gels, such as strong rigidity and brittleness, the konjac glucomannan, a natural polysaccharide, was added into AG hydrogels. After the addition of konjac glucomannan, it significantly reduces the hardness and rigidity of AG hydrogels [16]. However, the report found that cells encapsulated in AG hydrogels containing chondroitin sulfate and chondroitin sulfate graft copolymer showed lower metabolic activity and viability [17]. On the contrary, silk fibroin (SF), is a natural fibrous protein, shows excellent biocompatibility. The SF and hyaluronic acid blended hydrogels prepared via sonication can support encapsulation of human chondrocytes. Meanwhile, these SF–hyaluronic acid hydrogels had controllable gelation, degradation rates, and predictive temporal stiffening, and these characteristics were better than those of other natural polymer-based systems [18]. There are some novel applications that silk sponge system mimicking the structure of the bone marrow for in vivo production of functional platelets was proposed, which have improved the platelet yield [19]. However, the preparation of these hydrogels is time consuming. Although it was reported that sophorolipids can accelerate the gelation of SF to produce functional hydrogels, the gelation commences after 10 h. Thus, shortening the gelation time of SF is necessary [20].

To prevent wound infection, researchers have designed antibacterial hydrogels by incorporating antiseptics into dressings or using some constituents with inherent antibacterial activity, including an inorganic antibacterial agent, an organic antibacterial agent, and a natural antibacterial agent [21, 22]. Chitosan (CH) is a polycationic natural biopolymer with biocompatible and biodegradable ability [23]. It has proved antibacterial activity and antineoplastic activity [24]. Some studies have shown that CH can accelerate skin regeneration and reduce inflammation [25]. Moreover, only containing CH and water as fragmented physical hydrogel suspension, the promising new material could serve as a scaffold for spinal cord injury [26]. However, antibiotic-resistant bacteria tend to spread epidemically in hospitals and often lead to wound infections; this reduces the efficacy of antibiotic-loaded CH dressings in the application of infected wound care [27]. Thus, some effective antimicrobials used to treat wound infections caused by multidrug-resistant (MDR) bacteria are developed [28]. Silver nanoparticles (SNPs), as a frequently used inorganic antiseptic, have many advantages, including broad-spectrum antimicrobial activity, heat resistance, and inhibitory activity to drug-resistant bacteria. Introduction of SNPs into polyelectrolyte complexes systems is a desirable approach to fabricate biomaterials. The nano Ag/ZnO-loaded 2% CH composite dressing was prepared. In vitro and in vivo antibacterial studies proved its high antibacterial activities and faster wound healing [29]. On the other hand, to be more environment friendly, the free radical polymerization method, a green approach, was adopted to prepare nanosilver composite hydrogels [30]. Nevertheless, the overuse of SNPs may induce cell cytotoxicity [31]. To fabricate sound hydrogels doped with SNPs, the control of SNPs' concentration is very important and more green methods should be carried out.

In this research, we aim to develop a novel hydrogel that has both advantages of excellent mechanical and antibacterial properties by using AG, CH, SF, and SNPs. AG helps to form hydrogels and control their mechanical properties. CH is used as an antiseptic and a fortifier. The role of SF is to enhance biological activity. Meanwhile, SNPs, as an antibacterial agent, were capped into hydrogels for enhancing antibacterial activity. These novel hydrogels only experience an instantaneous gelation time. Moreover, the physicochemical properties, such as swelling behavior and structural conformation, mechanical property, and the constitution of the blended hydrogels were studied and the controllable mechanical property was proved. Furthermore, the optimized hydrogels were characterized for the antibacterial property, cell proliferation, and biocompatibility in hope that the system can improve biological response and accelerate wound healing by using SF, AG, CH, and SNPs as materials.

Results and discussion

Morphological analysis of hydrogels

The fabricated hydrogels are transparent in the hydrated state without any phase separation [Fig. 1(b)]. After freeze drying, the microstructure of hydrogels was observed by scanning electron microscope (SEM), which revealed the porous structure in all fabricated hydrogels [Fig. 2(a)]. The pore size of hydrogels with 0.5% AG is smaller than that of 0.25% AG hydrogels, and this may attribute to a firm structure. The further Energy Dispersive Spectrometer (EDS) investigation indicates that SNPs were blended into hydrogels.

Porosity analysis

The porous structure is a typical feature of hydrogels. Large porosity is able to promote cell proliferation and adhesion. The porosity of all hydrogels valued by the liquid displacement method without any volume change after the tests indicated the blended hydrogels have a good porosity, which can reach as high as 85%. This large porosity may contribute to absorbing more fluid exudate (Fig. 3). With the increased concentration of AG, the porosity of hydrogels increased. The introduction of CH also attributes to the increased hydrogels' porosity. This is because that CH is a positively charged alkaline polysaccharide, so that it possibly binds to SF through the electrostatic effect and hydrogen bonding. Besides, SNPs had a little effect on the porosity of hydrogels.

https://doi.org/10.1557/jmr.2019.77 Published online by Cambridge University Press

© Materials Research Society 2019

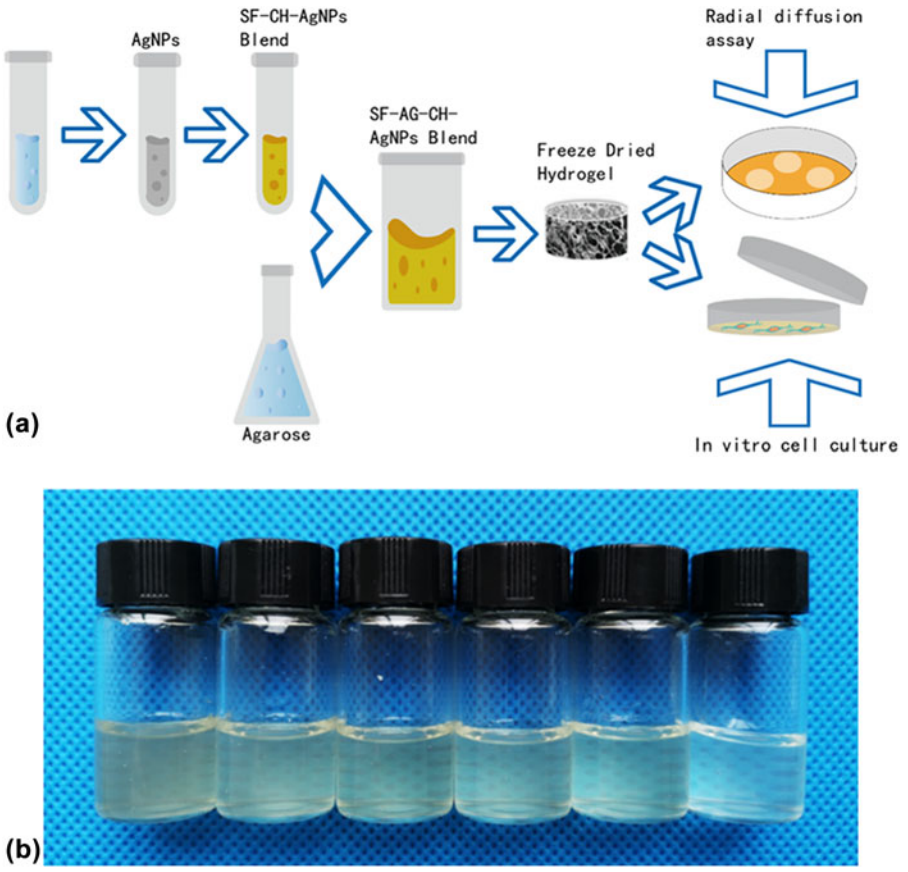


Figure 1: (a) Schematic representation of fabrication of hydrogels and (b) macroscopic appearance of the hydrogels.

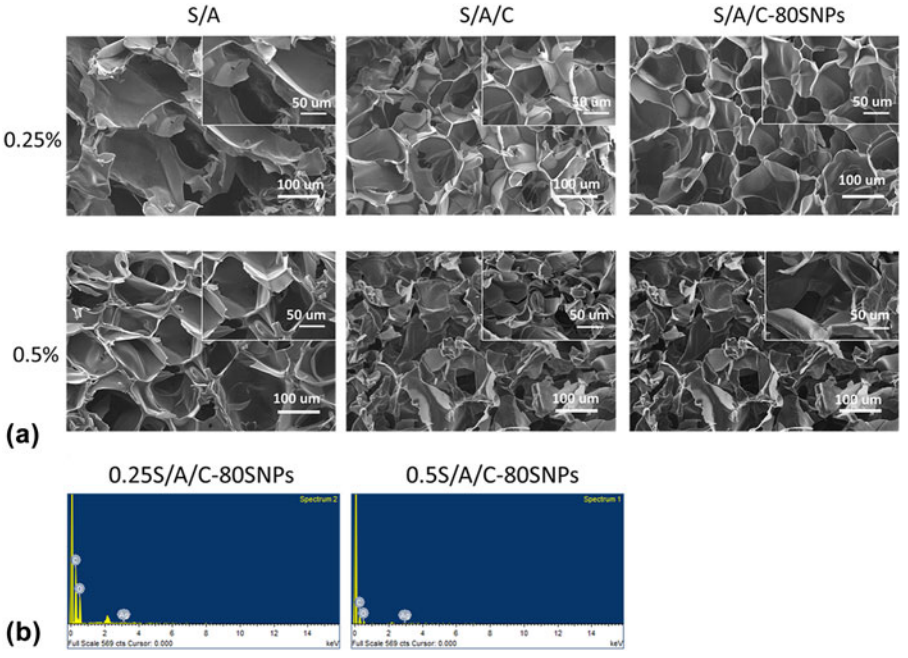


Figure 2: (a) SEM images of hydrogels with different magnification. Scale bar represents 100 μm. The scale bar of inset images represents 50 μm. (b) EDS images of S/A/C-80SNPs.

https://doi.org/10.1557/jmr.2019.77 Published online by Cambridge University Press

© Materials Research Society 2019

Swelling behavior

Adsorption and holding large amounts of water is basic to three-dimensional networks such as hydrogels. Thus, the valuation of their swelling ability is essential. The fabricated hydrogels after being immersed in ultrapure water at room temperature and weighed at a predefined time are shown in Fig. 4. All samples reached the equilibrium within 160 min. The rapid swelling was observed within the first 20 min, with a swelling ratio of 50%. The swelling ratio of 0.5S/A hydrogel was higher than that of 0.25S/A, which may result from the increased concentration of AG. And higher swelling (~1.4 times) was observed in hydrogels with CH. Meanwhile, a swelling equilibrium is delayed. Based on these results, it is reasonable to assume that the swelling behavior of a matrix is intrinsic to polymer properties and not dependent on pore size alone. Besides, the lower swelling was observed in hydrogels with SNPs, and varied concentrations of SNPs have a small effect on swelling behavior.

Mechanical property analysis

These developed hydrogels are intended to be used for wound dressing and cartilage repair; thus, their compressive property is of importance. The suitable hydrogels must be able to endure

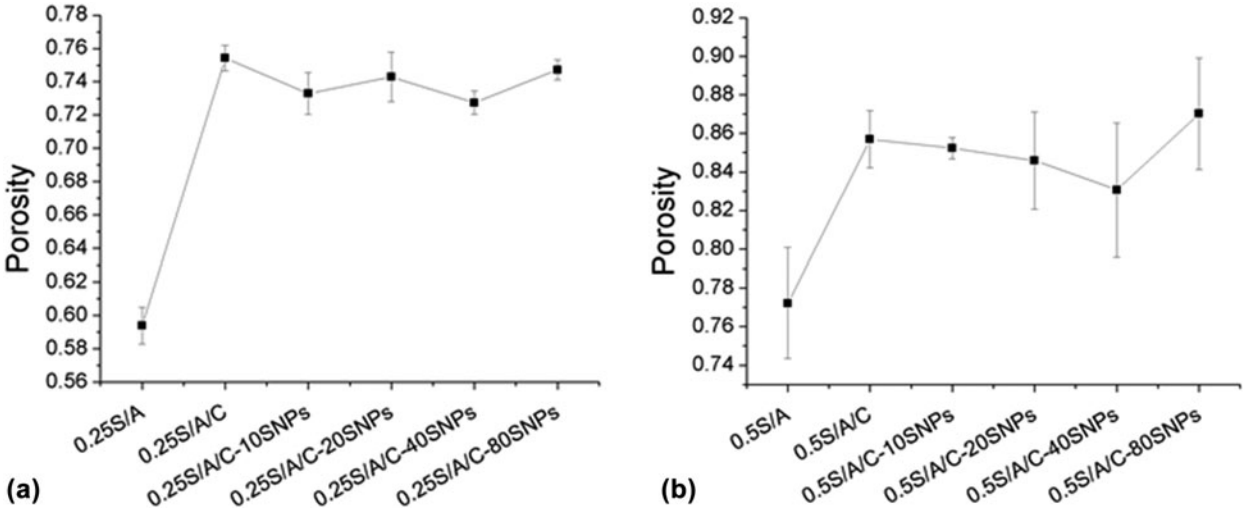


Figure 3: Porosity images of (a) 0.25% AG blended gels and (b) 0.5% AG blended gels.

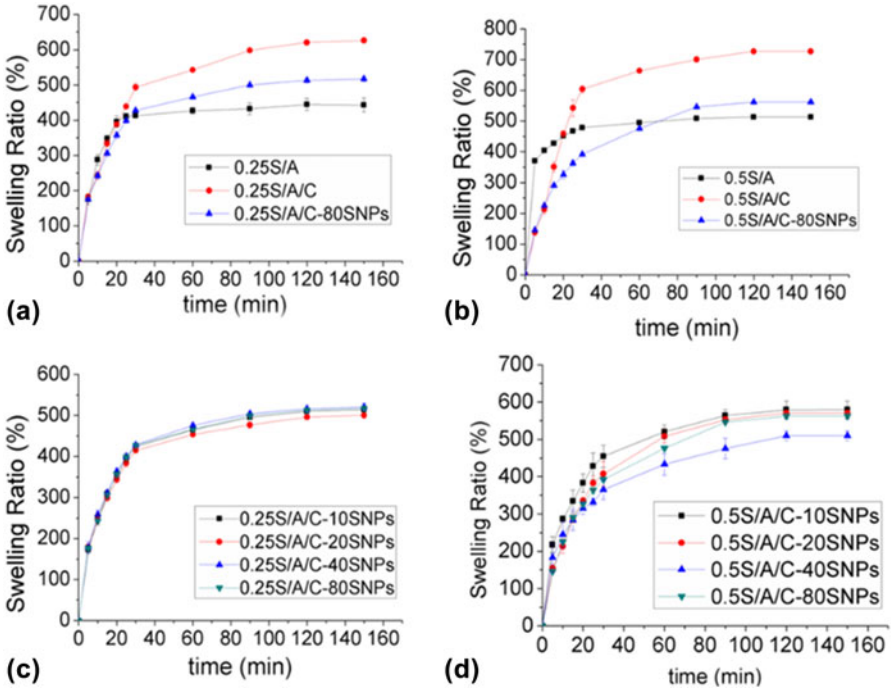


Figure 4: Swelling ratio of (a) 0.25% AG blended gels with different components, (b) 0.5% AG blended gels with different components, (c) 0.25S/A/C gels loaded varied SNPs and (d) 0.5S/A/C gels loaded varied SNPs in ultrapure water at 25 °C.

https://doi.org/10.1557/jmr.2019.77 Published online by Cambridge University Press

© Materials Research Society 2019

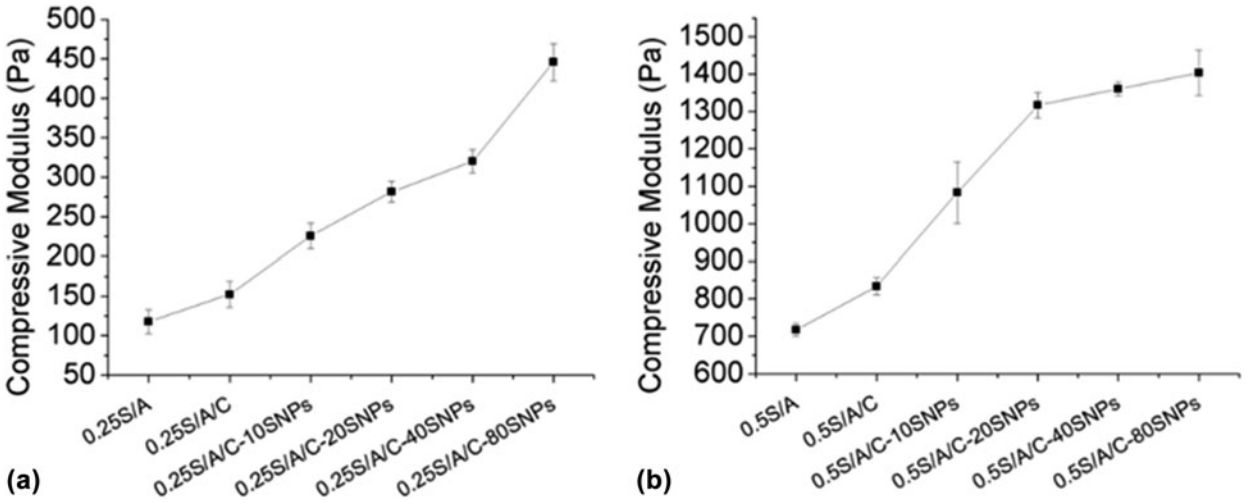


Figure 5: Compressive property of all samples, including (a) 0.25% AG blended gels and (b) 0.5% AG blended gels.

certain pressure during trivial movement. The investigation by an electromechanical universal testing machine indicated that the compressive modulus of gels increases 6 times with an increase in the concentration of AG from 0.25 to 0.5% (Fig. 5). And CH also can improve mechanical properties. The effect of SF on the strength of the resulting gels can attribute to the interaction between SF and CH as well as the structural characteristics of SF itself, as followed to be discussed, and forming interpenetrating polymer networks [32]. However, SNPs are known to have various reinforced effects on polymer composites. Figure 5 indicates compressive modulus of hydrogels with varied concentration of SNPs; it can be inferred that the enhanced strength is related to the effects of SNPs. When hydrogels were doped with 80 mg/L SNPs, the compressive modulus could reach to about 1371 Pa, which is higher (~1.8 times) than that of S/A gels. These results demonstrate that the mechanical properties can be regulated by adjusting the concentration of AG, CH, and SNPs. The 0.5% AG blended hydrogels with good mechanical performance were utilized for the further study.

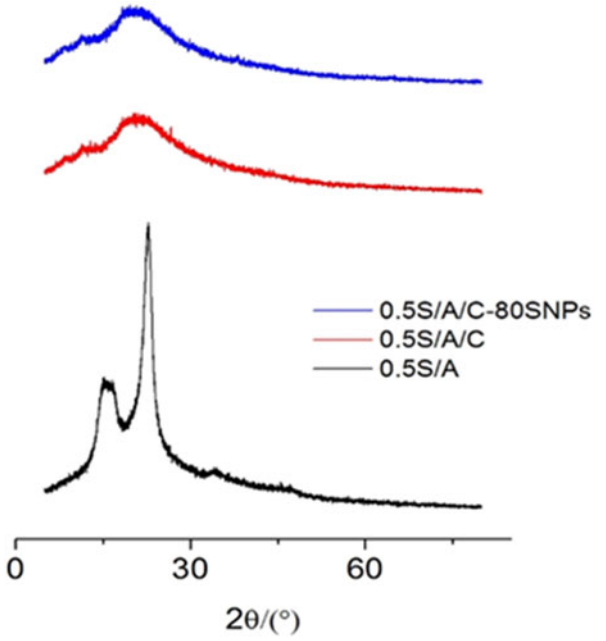


Figure 6: XRD patterns of 0.5S/A, 0.5S/A/C, and 0.5S/A/C-80SNPs.

X-ray powder diffraction analysis

The structural conformation of the fabricated hydrogels using X-ray powder diffraction (XRD) spectra is shown in Fig. 6. There were two typical peaks around 10° and 24° for S/A samples. These peaks were almost the same as those of the β-sheet crystalline structure of SF [33, 34]. A broad peak was observed at around 20° for both S/A/C and S/A/C-80SNPs samples, indicating an amorphous structure of SF [35]. From the results of X-ray diffraction, it was found that blended CH in gels induced a conformational transition from β-sheet into the random coil as previously reported [36]. Obtuse and broad peaks appeared when CH was added into hydrogels, which indicated that strong hydrogen bonding interaction occurred between SF and CH molecules [37]. This is to say, the introduction of CH leads to the formation of more hydrogen bond with SF. The good molecular level interaction would favor the formation of molecular level miscible polymer blend system and interchain entanglement.

Rheological characterization

The rheological behavior of hydrogels is shown in Fig. 7. The reports indicate that a strain of 5% was chosen for frequency sweep tests, because it was clear in the linear viscoelastic region of all hydrogels [38]. The frequency sweep revealed G' to be

https://doi.org/10.1557/jmr.2019.77 Published online by Cambridge University Press

© Materials Research Society 2019

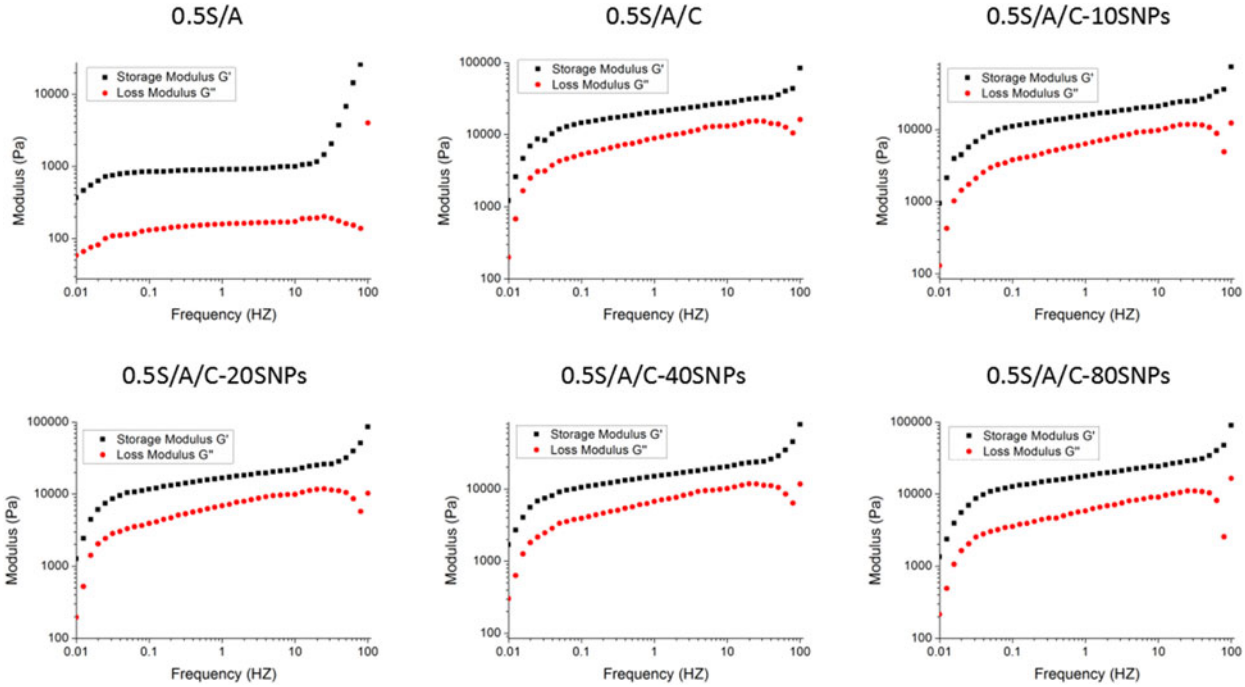


Figure 7: Frequency sweep of hydrogels displays the storage modulus (G') and loss modulus (G'').

TABLE I: Storage modulus (G'), loss modulus (G''), and loss angle (tan δ) of the 0.5% agarose blended hydrogels.

	S/A	S/A/C	S/A/C-10SNPs	S/A/C-20SNPs	S/A/C-40SNPs	S/A/C-80SNPs
G' (kPa)	0.85	14.5	11.06	11.68	10.50	12.68
G'' (kPa)	0.12	5.3	3.8	3.93	3.91	3.55
tan δ	0.13	0.37	0.34	0.34	0.37	0.28

higher than G'' in all hydrogels, which revealed that all hydrogels are stable at solid state although CH blended hydrogels are relatively stronger than S/A hydrogels. At a fixed frequency of 0.1 Hz for the hydrogels, Table I displays G', G'', and the loss angle (tan $\delta = G''/G'$) data. The modulus of CH blended hydrogels was higher than that of S/A hydrogels, reaching 1.5×10^4, which indicates a positive strengthening of the hydrogels on introducing CH. Furthermore, the loss angle for all the hydrogels was between 0.13 and 0.37, indicating that hydrogels are of solid-dominating nature along with a liquid component [39]. Goff et al. showed that the nanowhisker-filled hydrogels are a more fragile system [40]. It is the same as our results that modulus decreases when SNPs was introduced into hydrogels. The storage modulus of hydrogels was improved effectively by CH, indicating a higher cross-linking degree compared with S/A hydrogels.

Microbiological activity

The antibacterial activity of the fabricated dressings against gram-positive bacteria *Staphylococcus aureus* and gram-negative bacteria *Escherichia coli* was tested by an inhibition zone method, and the results are shown in Fig. 8(a). The S/A/C-SNPs with varied concentrations of SNPs exhibited antibacterial activities toward *S. aureus* and *E. coli*, while the S/A/C exhibits a little effect toward *S. aureus* and *E. coli*. This is possible because the antimicrobial effect decreased as the M_W of CH increased. It is reported that CH of lower M_W enters the microbial cell more easily, which disturbs the metabolism of the cell [41]. Nevertheless, the hydrogels doped with SNPs exhibited antimicrobial properties. The diameter of the inhibition zones for the varied concentrations of SNPs composite hydrogels are as follows: S/A/C-10SNPs < S/A/C-20SNPs < S/A/C-40SNPs < S/A/C-80SNPs, as is shown in Fig. 8(a). For the S/A/C-40SNPs and S/A/C-80SNPs groups, the clearer inhibition zones were observed; furthermore, for S/A/C-80SNPs, the larger inhibition zones indicated stronger antibacterial activity. The introduction of SNPs could obviously improve antibacterial ability, indicating that after releasing from the hydrogels, SNPs interact with sulfur-containing proteins in the bacterial membrane as well as with the phosphorus-containing compounds like DNA, before attacking the respiratory chain, finally leading to bacterial death

https://doi.org/10.1557/jmr.2019.77 Published online by Cambridge University Press

© Materials Research Society 2019

[42]. Moreover, S/A/C-80SNPs gels with excellent antimicrobial property were chosen for viability staining, as shown in Fig. 8(b). Membrane damage was monitored using fluorescent dyes and fluorescence microscopy. Bacteria with intact cell membranes stain fluorescent green, whereas bacteria with damaged membranes stain fluorescent red. As shown, none treated and S/A-treated bacteria exhibited great green fluorescence. Nevertheless, S/A/C- and S/A/C-80SNP-treated bacteria exhibited very little green fluorescence and large amounts of red fluorescence. Compared with the inhibition zone method, S/A/C-80SNPs gels also showed strong damage to *E. coli* and *S. aureus*. A large amount of red fluorescence was observed when bacteria were treated with S/A/C-80SNPs. It was revealed that dressings blended into 80 mg/mL SNPs have a stronger antibacterial effect than dressings only blended into CH.

Biocompatibility evaluation of hydrogels

Cell viability of the prepared blended hydrogels on L929 fibroblasts is shown in Fig. 9(a). After 24 h incubation, the S/A hydrogel obviously enhanced the growth of L929 cells. Although the cell viability treated with S/A/C gels and S/A/C-SNPs gels were decreased, all the hydrogels showed more than 85% of cell viability compared with non-treated group. The hydrogels containing different SNPs did not show significant toxicity at tested concentration, suggesting they are suitable for further wound dressing. The increase in SNP content has no influence on the toxicity, and the figure was consistent with the LIVE/DEAD staining results, which is shown in Fig. 9(b). Calcein is well retained within live cells, producing an intense uniform green fluorescence in live cells and EthD-1 enters cells with damaged membranes, producing

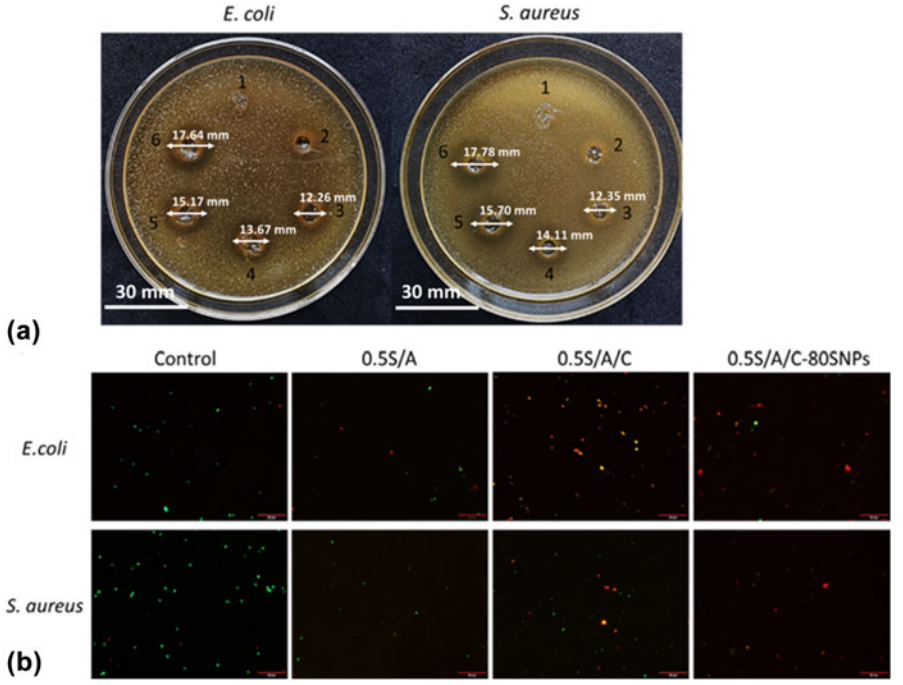


Figure 8: Microbiological activity of the hydrogels. (a) Inhibition zone diameters of *E. coli* and *S. aureus*. 1–6 represents S/A, S/A/C, S/A/C-10SNPs, S/A/C-20SNPs, S/A/C-40SNPs, and S/A/C-80SNPs. (b) Viability staining of *E. coli* and *S. aureus*. The white scale bar represents 30 mm and the red scale bar represents 50 μm.

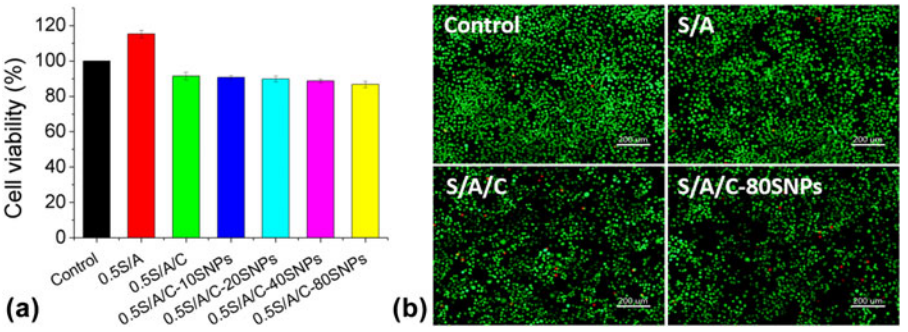


Figure 9: Biocompatibility evaluation of hydrogels including (a) MTT test and (b) LIVE/DEAD staining. The scale bar represents 200 μm.

https://doi.org/10.1557/jmr.2019.77 Published online by Cambridge University Press

© Materials Research Society 2019

a bright red fluorescence in dead cells. The cells in S/A/C-SNPs hydrogel group were green and showed a fusiform morphology similar to the control group. Few dead cells appeared in all groups because of cell metabolism. Both the cell viability and LIVE/DEAD staining results demonstrated that the hydrogels had good cytocompatibility.

Conclusion

In summary, the novel hydrogels made up of SF, AG, CH, and antibacterial agents like SNPs were fabricated via an efficient process, which directly doped SNPs into the composite hydrogel system. These novel hydrogels could gel immediately with benign reaction condition without any reductants or inorganic solutions. The mechanical tests revealed that with increasing AG content and doping CH and SNPs, mechanical performance would be improved. Thus, the mechanical property of hydrogels could be simply modulated by regulating the content of AG, CH, and SNPs. Meanwhile, the fabricated hydrogels displayed good swelling behavior and high porosity. The results of rheology showed that all hydrogels were stable in the solid state. In vitro antibacterial studies proved the high antibacterial activities against *E. coli* and *S. aureus*. Furthermore, indirect cytotoxicity assessment of the hydrogels with L929 fibroblasts indicated that it had good in vitro cellular compatibility, indicating that they are excellent candidates as bioactive materials for bioengineering.

Materials and methods

Materials

SF powder was purchased from Xi′an zelang Biotech Co., Ltd. (Xi′an, China). CH, 95% deacetylation degree, was purchased from Shanghai XinPing Fine Chemicals Co., Ltd. (Shanghai, China). AG was obtained from HydraGene Co., Ltd. (Xiamen, China). SNPs (purity: 99.99%, particle size: 20 nm) were acquired from HongWu New Material Co., Ltd. (Guangzhou, China). Dulbecco's modified Eagle's medium (DMEM), fetal bovine serum (FBS), trypsin–EDTA, and penicillin–streptomycin were acquired from Gibco BRL (Rockville, MD). MTT (3-(4,5-dimethylthiazol-2-yl)-2,5-diphenyltetrazolium bromide) Cell Proliferation and Cytotoxicity Assay Kit was acquired from Beyotime Biotechnology (Jiangsu, China). Viability/Cytotoxicity Assay Kit for Animal Live & Dead Cells was obtained from US Everbright Inc. (California) LIVE/DEAD BacLight Bacterial Viability Kit was purchased from Molecular Probes Inc. Other chemicals used were of analytical grade.

Preparation of the blended hydrogels

This novel SF/AG/CH-SNPs (coded as S/A/C-SNPs) was fabricated by addition of the dissolved AG solution to SF/AG solution containing with SNPs. The preparation scheme is shown in Fig. 1(a). The different concentrations of SNPs were dispersed in water to form homogeneous SNPs solution. And acetic acid was added into SNPs solution, offering an acidic environment. Then, 2% (w/v) CH and 5% (w/v) SF were mixed into the solution. Next, the varying levels of dissolved AG solution were added into the solution to form 0.25% and 0.5% (w/v) AG concentrations. The mixture was then transferred to a 48-well plate. And the mixture was cooled naturally to transform into blended hydrogels, then stored at 4 °C for further characterization. Then, the plate was frozen in a −20 °C refrigerator for 12 h and added to lyophilizer to fabricate lyophilized hydrogels, which are coded as 0.25S/A, 0.25S/A/C, 0.25S/A/C-10SNPs, 0.25S/A/C-20SNPs, 0.25S/A/C-40SNPs, and 0.25S/A/C-80SNPs, and 0.5% concentration AG coded as the same way. The macroscopic appearance of the blended hydrogels is presented in Fig. 1(b). The compositions of these solutions are also listed in Table II.

Morphological analysis of hydrogels

The surface morphology, pore size, and surface element were examined using an SEM (JSM-6610). The hydrogels were freeze-dried and sputter coated with gold, followed by scanning analysis at an accelerated electron energy of 15 kV.

Porosity analysis

To calculate the pore volume of the hydrogels, the liquid displacement method has been used. Briefly, a lyophilized hydrogel was immersed in anhydrous ethanol with the volume of V_1 and record the volume when hydrogel completely immersed in anhydrous ethanol, coded as V_2. After 10 min, the sample was taken out. The volume of the remaining anhydrous ethanol was coded as V_3. The experiments were conducted in sets of three ($N = 3$) under identical conditions, and porosity was calculated using the following equation:

$$P(\%) = (V_1 - V_3)/(V_2 - V_3) \times 100\% \quad .$$

Swelling behavior

To calculate the water uptake of the hydrogels, a conventional gravimetric method was adopted. Briefly, the dry weight of the hydrogels was recorded, coded as W_d, and then immersed in ultrapure water at room temperature until they achieved equilibrium. The swelled weight, coded as W_s, of hydrogels was taken at various time intervals. The experiments were conducted in sets of three ($N = 3$) under identical conditions, and the swelling ratio was calculated using the following equation:

$$\text{Swelling } (\%) = [(W_s - W_d)/W_d] \times 100\% \quad ,$$

where W_s is the swelled weight and W_d is the dry weight of the hydrogel.

https://doi.org/10.1557/jmr.2019.77 Published online by Cambridge University Press

© Materials Research Society 2019

TABLE II: Parameters of hydrogels.

Sample name[a]	Concentration of agarose (w/v %)	Concentration of SNPs (mg/L)	Concentration of chitosan (w/v %)	Compressive modulus (Pa)	Swelling ratio (g/g)
0.25S/A	0.25	...	...	134.92 ± 10	4.43 ± 0.13
0.25S/A/C	0.25	...	2.0	168.86 ± 12	6.26 ± 0.06
0.25S/A/C-10SNPs	0.25	10	2.0	216.82 ± 15	5.14 ± 0.09
0.25S/A/C-20SNPs	0.25	20	2.0	269.53 ± 9.2	5.00 ± 0.06
0.25S/A/C-40SNPs	0.25	40	2.0	334.06 ± 6.3	5.20 ± 0.12
0.25S/A/C-80SNPs	0.25	80	2.0	428.09 ± 22	5.17 ± 0.08
0.5S/A	0.5	...	...	716.47 ± 21	5.13 ± 0.31
0.5S/A/C	0.5	...	2.0	849.70 ± 18	7.26 ± 0.07
0.5S/A/C-10SNPs	0.5	10	2.0	1116.56 ± 35	5.62 ± 0.55
0.5S/A/C-20SNPs	0.5	20	2.0	1347.46 ± 22	5.09 ± 0.84
0.5S/A/C-40SNPs	0.5	40	2.0	1360.46 ± 14	5.70 ± 0.33
0.5S/A/C-80SNPs	0.5	80	2.0	1371.28 ± 41	5.79 ± 0.87

[a]The concentration of SF for all gel samples was 5%.

Mechanical property analysis

The compression test was carried out using Electromechanical Universal Testing Machine (E44. 104) to analyze the mechanical properties. The experiments were executed using a stainless steel (20 mm diameter) compression clamp. The compression test was carried out at a measurement speed of 1.6 mm/s at room temperature and the velocity coefficient is 0.5. All the experiments were conducted in sets of three ($N = 3$) under identical conditions, and the compressive modulus was calculated using the following equation:

$$\text{Compressive modulus} = F_b/S \quad ,$$

where F_b is the maximum breaking load and S is the surface area of compression clamp.

X-ray powder diffraction

An XRD study was carried out using an Bruker D8 Focus X-ray diffractometer (Duisburg, Germany) XRD measurements were recorded in the range of 5°–80°, with a speed rate of 5°/min and step length of 0.02. SNPs crystal structure was analyzed according to Joint Committee on Power Diffraction Standards (JCPDS) card.

Rheological characterization

Rheological measurements of the hydrogels were performed by using a TA DHR-2 rheometer (Dallas, TX) using frequency sweeps. The tests were executed using a stainless steel (25 mm diameter) parallel plate. For each measurement, the preformed hydrogel (20 mm diameter) was placed on the lower plate of the rheometer, and the gap between the plates was maintained at 4 mm. The frequency sweep was carried out in the range of 0.01–100 Hz at a constant strain of 5% to obtain storage modulus (G'), and loss modulus (G'').

Microbiological activity

Microbiological activity tests were all performed by beating hole method. Briefly, a well of 6 mm in diameter was punched in agar medium, then 60 μg of hydrogel was added to the hole. The microbiological tests were performed by the inhibition zone method. Two kinds of strains, including the model gram-positive bacteria *S. aureus* and the model gram-negative bacteria *E. coli*, were inoculated in Luria–Bertani medium. The plates were incubated for 24 h at 37 °C. Bacteria developed on agar medium, except in a clear zone around the disk samples. The radius of the clear zone around the disk samples was measured visually showing their antibacterial activity. The microbiological activity also evaluated by the SYTO 9 staining generally labels all bacteria in a population—those with intact membranes and those with damaged membranes, and propidium iodide penetrates only bacteria with damaged membranes. With 6 μM SYTO 9 stain and 30 μM propidium iodide, bacteria with intact cell membranes stain fluorescent green, whereas bacteria with damaged membranes stain fluorescent red.

Biocompatibility evaluation of hydrogels

The L929 fibroblasts were grown in DMEM containing 10% heat-inactivated FBS with 4.5 g/L D-glucose, 4 mM L-Glutamine, and 1% penicillin/streptomycin solution. The cells were kept under aseptic conditions at 37 °C and 5% CO_2. The media were refreshed every 2 days until the cells reached confluence. To evaluate the biocompatibility of hydrogels, a conventional extracting approach has been adopted. Briefly, samples were sterilized in 75% ethanol for 30 min and irradiated with ultraviolet radiation for another 15 min. Then the samples were immersed in complete medium at 37 °C for 24 h to attain extraction. And samples were stored at 4 °C to be used. Cell suspensions at 1×10^4 cells/mL concentration seeded in a 96-well plate culturing for 24 h. Then, 100 μL of extract was added to each well culturing another 24 h. After 10 μL of MTT solutions was added for 4 h. After 100 μL formazan was added for another 4 h. The absorbance at 570 nm was recorded by using a microplate reader (Sunrise Xfluor4). The control group containing cells was cultured without extracts. All experiments

https://doi.org/10.1557/jmr.2019.77 Published online by Cambridge University Press

© Materials Research Society 2019

were done at least in triplicate. The cell viability of the samples was calculated as follows:

$$\text{Cell viability} = \text{OD}_{570}(\text{sample})/\text{OD}_{570}(\text{control}) \times 100\% \quad ,$$

where the optical density (OD) values of the samples and the control are coded as OD_{570} (sample) and OD_{570} (control).

Cell viability also evaluated by the calcein AM and ethidium homodimer-1 (EthD-1). With 2 μM calcein AM and 4 μM EthD-1, the polyanionic dye calcein is well retained within live cells, producing an intense uniform green fluorescence in live cells and EthD-1 enters cells with damaged membranes and undergoes a 40-fold enhancement of fluorescence on binding to nucleic acids, thereby producing a bright red fluorescence in dead cells.

Acknowledgments

The research was supported by the Hi-Tech Research and Development 863 Program of China Grant (No. 2013AA102507), Funds of China Agriculture Research System (No. CARS-18-ZJ0102), and Chongqing Research Program of Basic Research and Frontier Technology (No. cstc2017jcyjAX0087).

References

1. **R. Xu, G. Luo, H. Xia, W. He, J. Zhao, B. Liu, J. Tan, J. Zhou, D. Liu, Y. Wang, Z. Yao, R. Zhan, S. Yang, and J. Wu**: Novel bilayer wound dressing composed of silicone rubber with particular micropores enhanced wound re-epithelialization and contraction. *Biomaterials* **40**, 1–11 (2015).
2. **C. Gong, Q. Wu, Y. Wang, D. Zhang, F. Luo, X. Zhao, Y. Wei, and Z. Qian**: A biodegradable hydrogel system containing curcumin encapsulated in micelles for cutaneous wound healing. *Biomaterials* **34**, 6377–6387 (2013).
3. **X. Zhao, H. Wu, B. Guo, R. Dong, Y. Qiu, and P.X. Ma**: Antibacterial anti-oxidant electroactive injectable hydrogel as self-healing wound dressing with hemostasis and adhesiveness for cutaneous wound healing. *Biomaterials* **122**, 34–47 (2017).
4. **A.R. Unnithan, G. Gnanasekaran, Y. Sathishkumar, Y.S. Lee, and C.S. Kim**: Electrospun antibacterial polyurethane-cellulose acetate-zein composite mats for wound dressing. *Carbohydr. Polym.* **102**, 884–892 (2014).
5. **S. MacNeil**: Progress and opportunities for tissue-engineered skin. *Nature* **445**, 874–880 (2007).
6. **S. Duchi, C. Onofrillo, C.D. O'Connell, R. Blanchard, C. Augustine, A.F. Quigley, R.M.I. Kapsa, P. Pivonka, G. Wallace, C. Di Bella, and P.F.M. Choong**: Handheld co-axial bioprinting: Application to in situ surgical cartilage repair. *Sci. Rep.* **7**, 5837 (2017).
7. **J.L. Drury and D.J. Mooney**: Hydrogels for tissue engineering: Scaffold design variables and applications. *Biomaterials* **24**, 4337–4351 (2003).
8. **G.P. Raeber, M.P. Lutolf, and J.A. Hubbell**: Molecularly engineered PEG hydrogels: A novel model system for proteolytically mediated cell migration. *Biophys. J.* **89**, 1374–1388 (2005).
9. **B.K. Mann, A.S. Gobin, A.T. Tsai, R.H. Schmedlen, and J.L. West**: Smooth muscle cell growth in photopolymerized hydrogels with cell adhesive and proteolytically degradable domains: Synthetic ECM analogs for tissue engineering. *Biomaterials* **22**, 3045–3051 (2001).
10. **T. Ngoc Quyen, Y.K. Joung, E. Lih, and K.D. Park**: In situ forming and rutin-releasing chitosan hydrogels as injectable dressings for dermal wound healing. *Biomacromolecules* **12**, 2872–2880 (2011).
11. **B. Balakrishnan, M. Mohanty, A.C. Fernandez, P.V. Mohanan, and A. Jayakrishnan**: Evaluation of the effect of incorporation of dibutyryl cyclic adenosine monophosphate in an in situ-forming hydrogel wound dressing based on oxidized alginate and gelatin. *Biomaterials* **27**, 1355–1361 (2006).
12. **J.Z. Yang, Y.S. Zhang, K. Yue, and A. Khademhosseini**: Cell-laden hydrogels for osteochondral and cartilage tissue engineering. *Acta Biomater.* **57**, 1–25 (2017).
13. **W. Li, X. Li, W. Li, T. Wang, X. Li, S. Pan, and H. Deng**: Nanofibrous mats layer-by-layer assembled via electrospun cellulose acetate and electrosprayed chitosan for cell culture. *Eur. Polym. J.* **48**, 1846–1853 (2012).
14. **S. Mohammed, G. Chouhan, O. Anuforom, M. Cooke, A. Walsh, P. Morgan-Warren, M. Jenkins, and F. de Cogan**: Thermosensitive hydrogel as an in situ gelling antimicrobial ocular dressing. *Mater. Sci. Eng., C* **78**, 203–209 (2017).
15. **V. Normand, D.L. Lootens, E. Amici, K.P. Plucknett, and P. Aymard**: New insight into agarose gel mechanical properties. *Biomacromolecules* **1**, 730–738 (2000).
16. **Y. Yuan, L. Wang, R.J. Mu, J.N. Gong, Y.Y. Wang, Y.Z. Li, J.Q. Ma, J. Pang, and C.H. Wu**: Effects of konjac glucomannan on the structure, properties, and drug release characteristics of agarose hydrogels. *Carbohydr. Polym.* **190**, 196–203 (2018).
17. **H.M. Pauly, L.W. Place, T.L.H. Donahue, and M.J. Kipper**: Mechanical properties and cell compatibility of agarose hydrogels containing proteoglycan mimetic graft copolymers. *Biomacromolecules* **18**, 2220–2229 (2017).
18. **N.R. Raia, B.P. Partlow, M. McGill, E.P. Kimmerling, C.E. Ghezzi, and D.L. Kaplan**: Enzymatically crosslinked silk-hyaluronic acid hydrogels. *Biomaterials* **131**, 58–67 (2017).
19. **L. Tozzi, P.A. Laurent, C.A. Di Buduo, X. Mu, A. Massaro, R. Bretherton, W. Stoppel, D.L. Kaplan, and A. Balduini**: Multi-channel silk sponge mimicking bone marrow vascular niche for platelet production. *Biomaterials* **178**, 122–133 (2018).

https://doi.org/10.1557/jmr.2019.77 Published online by Cambridge University Press

© Materials Research Society 2019

20. **P. Dubey, S. Kumar, V.K. Aswal, S. Ravindranathan, P.R. Rajamohanan, A. Prabhune, and A. Nisal**: Silk fibroin-sophorolipid gelation: Deciphering the underlying mechanism. *Biomacromolecules* **17**, 3318–3327 (2016).
21. **R. Gharibi, H. Yeganeh, A. Rezapour-Lactoee, and Z.M. Hassan**: Stimulation of wound healing by electroactive, antibacterial, and antioxidant polyurethane/siloxane dressing membranes: In vitro and in vivo evaluations. *ACS Appl. Mater. Interfaces* **7**, 24296–24311 (2015).
22. **W-Y. Chen, H-Y. Chang, J-K. Lu, Y-C. Huang, S.G. Harroun, Y-T. Tseng, Y-J. Li, C-C. Huang, and H-T. Chang**: Self-assembly of antimicrobial peptides on gold nanodots: Against multidrug-resistant bacteria and wound-healing application. *Adv. Funct. Mater.* **25**, 7189–7199 (2015).
23. **M. Dash, F. Chiellini, R.M. Ottenbrite, and E. Chiellini**: Chitosan-A versatile semi-synthetic polymer in biomedical applications. *Prog. Polym. Sci.* **36**, 981–1014 (2011).
24. **H. Ueno, T. Mori, and T. Fujinaga**: Topical formulations and wound healing applications of chitosan. *Adv. Drug Delivery Rev.* **52**, 105–115 (2001).
25. **R.R. Klossner, H.A. Queen, A.J. Coughlin, and W.E. Krause**: Correlation of chitosan's rheological properties and its ability to electrospin. *Biomacromolecules* **9**, 2947–2953 (2008).
26. **J. Chedly, S. Soares, A. Montembault, Y. von Boxberg, M. Veron-Ravaille, C. Mouffle, M.N. Benassy, J. Taxi, L. David, and F. Nothias**: Physical chitosan microhydrogels as scaffolds for spinal cord injury restoration and axon regeneration. *Biomaterials* **138**, 91–107 (2017).
27. **H. Pirvanescu, M. Balasoiu, M.E. Ciurea, A.T. Balasoiu, and R. Manescu**: Wound infections with multi-drug resistant bacteria. *Chirurgia* **109**, 73–79 (2014).
28. **D. Liang, Z. Lu, H. Yang, J. Gao, and R. Chen**: Novel asymmetric wettable AgNPs/chitosan wound dressing: In vitro and in vivo evaluation. *ACS Appl. Mater. Interfaces* **8**, 3958–3968 (2016).
29. **Z. Lu, J. Gao, Q. He, J. Wu, D. Liang, H. Yang, and R. Chen**: Enhanced antibacterial and wound healing activities of microporous chitosan-Ag/ZnO composite dressing. *Carbohydr. Polym.* **156**, 460–469 (2017).
30. **T. Jayaramudu, K. Varaprasad, G.M. Raghavendra, E.R. Sadiku, K. Mohana Raju, and J. Amalraj**: Green synthesis of tea Ag nanocomposite hydrogels via mint leaf extraction for effective antibacterial activity. *J. Biomater. Sci., Polym. Ed.* **28**, 1588–1602 (2017).
31. **M. Ahamed, M.S. AlSalhi, and M.K.J. Siddiqui**: Silver nanoparticle applications and human health. *Clin. Chim. Acta* **411**, 1841–1848 (2010).
32. **P. Matricardi, C. Di Meo, T. Coviello, W.E. Hennink, and F. Alhaique**: Interpenetrating polymer networks polysaccharide hydrogels for drug delivery and tissue engineering. *Adv. Drug Delivery Rev.* **65**, 1172–1187 (2013).
33. **Z.H. Ayub, M. Arai, and K. Hirabayashi**: Mechanism of the gelation of fibroin solution. *Biosci., Biotechnol., Biochem.* **57**, 1910–1912 (1993).
34. **T. Asakura, A. Kuzuhara, R. Tabeta, and H. Saito**: Conformation characterization of bombyx mori silk fibroin in the solid state by high-frequency 13c cross polarization–magic angle spinning NMR, X-ray diffraction, and infrared spectroscopy. *Macromolecules* **18**, 1841–1845 (1985).
35. **J. Magoshi, Y. Magoshi, M.A. Becker, and S. Nakamura**: Biospinning by bombyx mori silkworm. *Abstr. Pap.* **212**, 53-CELL (1996).
36. **T. Hanawa, A. Watanabe, T. Tsuchiya, R. Ikoma, M. Hidaka, and M. Sugihara**: New oral dosage form for elderly patients—preparation and characterization of silk fibroin gel. *Chem. Pharm. Bull.* **43**, 284–288 (1995).
37. **Y. Zhou, Q. Dong, H. Yang, X. Liu, X. Yin, Y. Tao, Z. Bai, and W. Xu**: Photocrosslinked maleilated chitosan/methacrylated poly(vinyl alcohol) bicomponent nanofibrous scaffolds for use as potential wound dressings. *Carbohydr. Polym.* **168**, 220–226 (2017).
38. **Y.P. Singh, N. Bhardwaj, and B.B. Mandal**: Potential of agarose/silk fibroin blended hydrogel for in vitro cartilage tissue engineering. *ACS Appl. Mater. Interfaces* **8**, 21236–21249 (2016).
39. **M.V. Priya, R.A. Kumar, A. Sivashanmugam, S.V. Nair, and R. Jayakumar**: Injectable amorphous chitin-agarose composite hydrogels for biomedical applications. *J. Funct. Biomater.* **6**, 849–862 (2015).
40. **K.J. Le Goff, C. Gaillard, W. Helbert, C. Garnier, and T. Aubry**: Rheological study of reinforcement of agarose hydrogels by cellulose nanowhiskers. *Carbohydr. Polym.* **116**, 117–123 (2015).
41. **L.Y. Zheng and J.A.F. Zhu**: Study on antimicrobial activity of chitosan with different molecular weights. *Carbohydr. Polym.* **54**, 527–530 (2003).
42. **M. Rai, A. Yadav, and A. Gade**: Silver nanoparticles as a new generation of antimicrobials. *Biotechnol. Adv.* **27**, 76–83 (2009).

https://doi.org/10.1557/jmr.2019.77 Published online by Cambridge University Press

© Materials Research Society 2019